

e e e e % e e 1 e e 1 e
e e e e e e e ()
1 e e e e e e e

& 10003, 210016,
e 36 4 -5305.

(Received 1 January 2015; accepted 4 April 2016; first published online 1 May 2016)

1. I 7

~~† t... e e 1 e ee e / 1.6 / 1.e~~

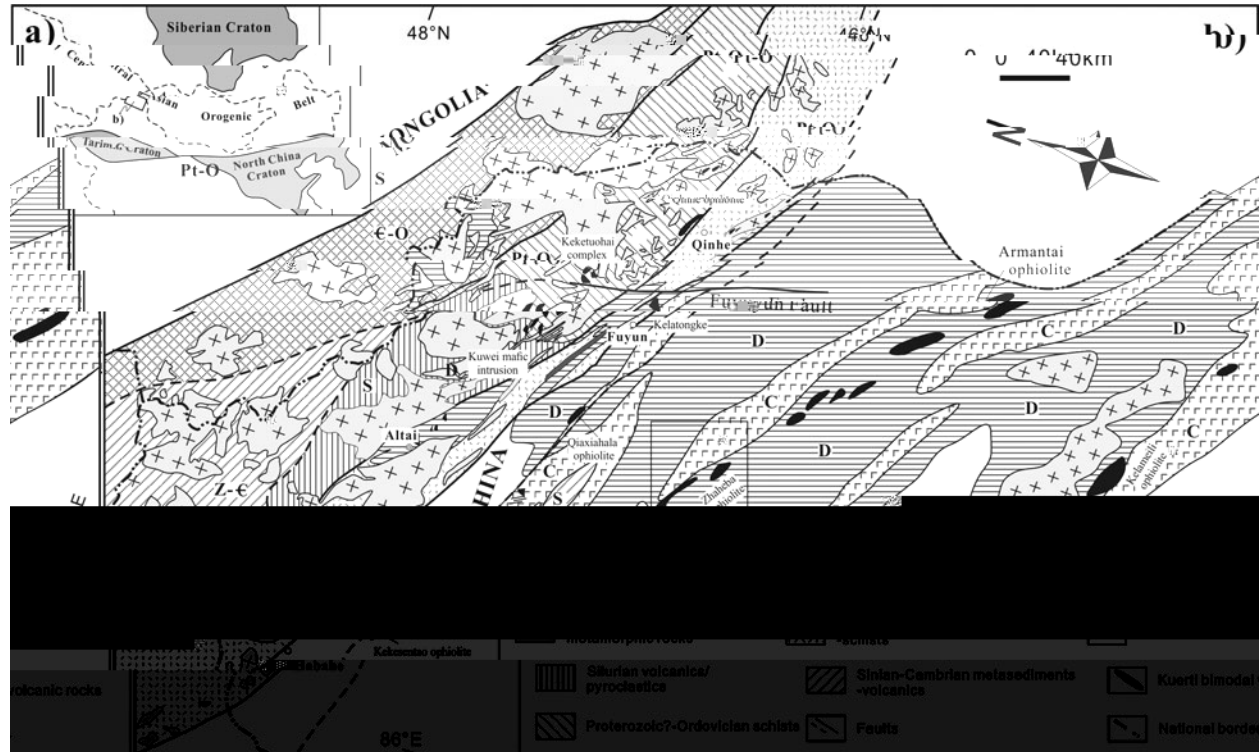


Fig. 1. (a) Regional geological map of Mongolia and surrounding regions (modified after *et al.* 2000).

the central part of the belt, the 1.1–1.0% $\delta^{13}\text{C}_{\text{PDB}}$ values are higher than those in the eastern part, reaching up to 1.1‰. The 1.1–1.0‰ $\delta^{13}\text{C}_{\text{PDB}}$ values are observed in the eastern part of the belt, which is consistent with the results of previous studies (Li *et al.* 2000; Li *et al.* 2006).

2. Regional geological setting

The geological setting of the northern part of the belt is characterized by the presence of the Keketuohai ophiolite, which is a typical example of the continental margin ophiolite system (Li *et al.* 2000; Li *et al.* 2006). The ophiolite is composed of ultramafic rocks, gabbros, and serpentinites, and it is surrounded by metamorphic rocks and metasediments. The ophiolite is overlain by a thick sequence of metasediments and metavolcanic rocks, which are interpreted as being derived from a continental margin environment. The ophiolite is also associated with a series of mafic intrusions, such as the Kuwei mafic intrusion, which is located to the west of the ophiolite. The ophiolite is bounded to the east by the Fuyun-Dun fault, which is a major tectonic feature in the region. The ophiolite is also associated with a series of mafic intrusions, such as the Kuwei mafic intrusion, which is located to the west of the ophiolite. The ophiolite is bounded to the east by the Fuyun-Dun fault, which is a major tectonic feature in the region.

The southern part of the belt is characterized by the presence of the Quaxihala ophiolite, which is a typical example of the continental margin ophiolite system (Li *et al.* 2000; Li *et al.* 2006). The ophiolite is composed of ultramafic rocks, gabbros, and serpentinites, and it is surrounded by metamorphic rocks and metasediments. The ophiolite is overlain by a thick sequence of metasediments and metavolcanic rocks, which are interpreted as being derived from a continental margin environment. The ophiolite is also associated with a series of mafic intrusions, such as the Kuwei mafic intrusion, which is located to the west of the ophiolite. The ophiolite is bounded to the east by the Fuyun-Dun fault, which is a major tectonic feature in the region. The ophiolite is also associated with a series of mafic intrusions, such as the Kuwei mafic intrusion, which is located to the west of the ophiolite. The ophiolite is bounded to the east by the Fuyun-Dun fault, which is a major tectonic feature in the region.

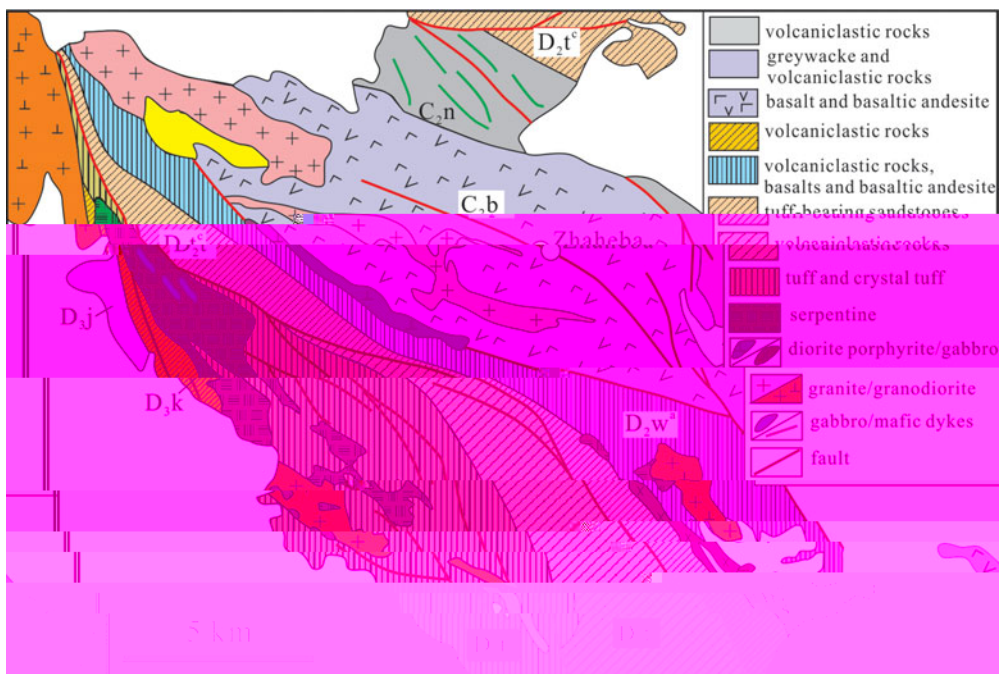


Fig. 2. (a) Geological sketch of the Zhaheba ophiolite showing major structural zones and main lithologies (modified after Li et al. 2005, 2006; Wang et al. 2006; Li & Wang, 2008).

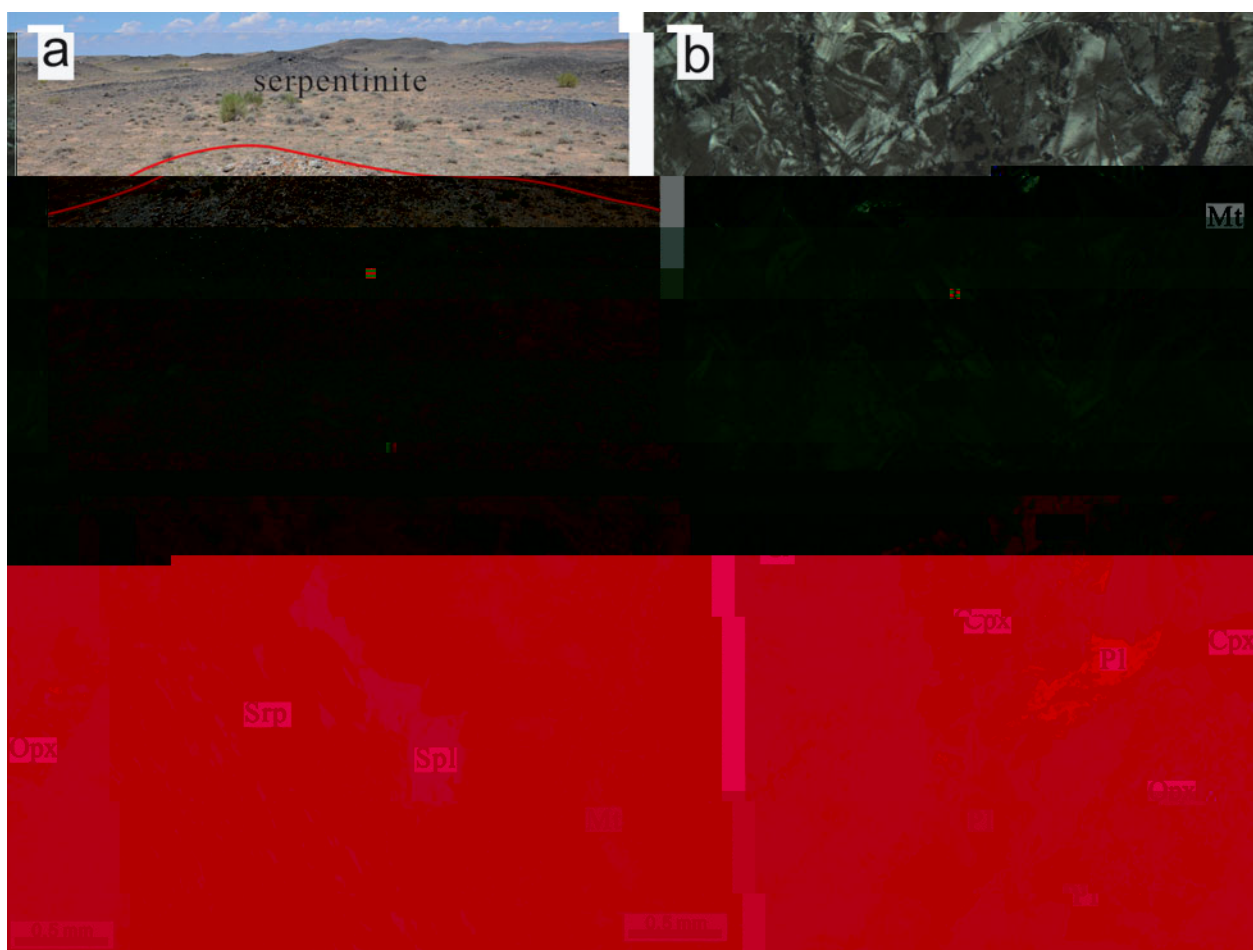


Fig. 3. (a) Photograph of serpentinite and its cathodoluminescence (CL) image showing olivine (Opx) and spinel (Sp) inclusions. (b) Photograph and CL image of olivine (Opx) and magnesian olivine (Mt) in the Zhaheba ophiolite.

the Zr/U ratio is 1.00 ± 0.00, and the Pb/U ratio is 1.00 ± 0.00.

3. Analysis

3.a. Zr-U-Pb dating

The zircon U-Pb ages were obtained from 10 samples (2013-01, 46°32'51"S, 24°11"E; 2013-02, 46°33'21"S, 24°23"E) using the ID-TIMS method at the Institute of Geology and Mineral Resources, Chinese Academy of Geological Sciences (Wang et al., 2004). The analytical conditions are as follows: heating temperature, 1000°C; heating time, 1 min; heating rate, 10°C/min; cooling rate, 10°C/min; sample size, 100 µg; counting time, 1000 s; blank value, 1000 ppm; detection limit, 100 ppm. The analytical results are shown in Table 1. The concordia diagram shows that the samples are concordant, with an overall concordance of 95% (Fig. 1). The weighted mean age of the samples is 11.1 ± 0.2 Ma (n = 10, 95% confidence interval), which is consistent with the age of the samples (11.1 ± 0.2 Ma) obtained by the Rb-Sr method (Wang et al., 2011).

3.b. Major element analysis

The major element compositions of the samples are listed in Table 1. The samples have a low CaO content (0.00–1.00%), a high Na2O content (1.00–11.00%), and a low K2O content (0.00–1.00%). The samples are enriched in LREEs and depleted in HREEs, with a positive Eu anomaly (Eu/Eu* = 1.15–1.15).

The Zr/Nb ratio is 20.0 ± 1.0, the Yb/Nb ratio is 1.1 ± 0.1, the Ce/Nb ratio is 4.5 ± 0.5, and the La/Nb ratio is 1.11 ± 0.01.

3.c. Whole-rock geochemistry

The whole-rock geochemical data are shown in Table 2. The samples are enriched in LREEs and depleted in HREEs, with a positive Eu anomaly (Eu/Eu* = 1.1–1.2). The samples have a low $\text{Mg}^{#}$ value (1.1–1.2), a high $\text{CaO}/\text{Al}_2\text{O}_3$ ratio (1.3–1.5), and a low SiO_2 content (60.00–61.00%). The samples are enriched in $\text{K}_{2\text{O}}$ and $\text{Na}_{2\text{O}}$ and depleted in TiO_2 , V_{2O_5} , and Cr_{2O_3} . The samples have a low $\text{Mg}^{#}$ value and a high $\text{CaO}/\text{Al}_2\text{O}_3$ ratio, indicating a high degree of differentiation.

The $\text{Mg}^{#}$ values of the samples range from 1.1 to 1.2, and the $\text{CaO}/\text{Al}_2\text{O}_3$ ratios range from 1.3 to 1.5. The SiO_2 contents of the samples range from 60.00 to 61.00%. The $\text{K}_{2\text{O}}/\text{Na}_{2\text{O}}$ ratios range from 0.11 to 0.14, and the $\text{Na}_{2\text{O}}/\text{CaO}$ ratios range from 0.102 to 0.143. The $\text{Mg}^{#}$ values of the samples are calculated using the formula $\text{Mg}^{#} = \text{Mg}/(\text{Mg} + \text{Fe})$ (Figs. 2a–2c). The $\text{CaO}/\text{Al}_2\text{O}_3$ ratios of the samples are calculated using the formula $\text{CaO}/\text{Al}_2\text{O}_3 = \text{CaO}/(2\text{Al}_2\text{O}_3)$ (Figs. 2d–2f). The SiO_2 contents of the samples are calculated using the formula $\text{SiO}_2 = \text{SiO}_2/\text{SiO}_2 + \text{Al}_2\text{O}_3 + \text{FeO} + \text{MgO}$ (Figs. 2g–2i). The $\text{K}_{2\text{O}}/\text{Na}_{2\text{O}}$ ratios of the samples are calculated using the formula $\text{K}_{2\text{O}}/\text{Na}_{2\text{O}} = \text{K}_{2\text{O}}/\text{Na}_{2\text{O}} + \text{K}_{2\text{O}}/\text{Na}_{2\text{O}} + \text{K}_{2\text{O}}/\text{Na}_{2\text{O}}$ (Figs. 2j–2l). The $\text{Na}_{2\text{O}}/\text{CaO}$ ratios of the samples are calculated using the formula $\text{Na}_{2\text{O}}/\text{CaO} = \text{Na}_{2\text{O}}/\text{CaO} + \text{Na}_{2\text{O}}/\text{CaO} + \text{Na}_{2\text{O}}/\text{CaO}$ (Figs. 2m–2o). The $\text{Mg}^{#}$ values of the samples are calculated using the formula $\text{Mg}^{#} = \text{Mg}/(\text{Mg} + \text{Fe})$ (Figs. 2p–2r). The $\text{CaO}/\text{Al}_2\text{O}_3$ ratios of the samples are calculated using the formula $\text{CaO}/\text{Al}_2\text{O}_3 = \text{CaO}/(2\text{Al}_2\text{O}_3)$ (Figs. 2s–2t). The SiO_2 contents of the samples are calculated using the formula $\text{SiO}_2 = \text{SiO}_2/\text{SiO}_2 + \text{Al}_2\text{O}_3 + \text{FeO} + \text{MgO}$ (Figs. 2u–2v). The $\text{K}_{2\text{O}}/\text{Na}_{2\text{O}}$ ratios of the samples are calculated using the formula $\text{K}_{2\text{O}}/\text{Na}_{2\text{O}} = \text{K}_{2\text{O}}/\text{Na}_{2\text{O}} + \text{K}_{2\text{O}}/\text{Na}_{2\text{O}} + \text{K}_{2\text{O}}/\text{Na}_{2\text{O}}$ (Figs. 2w–2x). The $\text{Na}_{2\text{O}}/\text{CaO}$ ratios of the samples are calculated using the formula $\text{Na}_{2\text{O}}/\text{CaO} = \text{Na}_{2\text{O}}/\text{CaO} + \text{Na}_{2\text{O}}/\text{CaO} + \text{Na}_{2\text{O}}/\text{CaO}$ (Figs. 2y–2z).

4. Analysis

4.a. Zr-U-Pb dating

The zircon U-Pb ages were obtained from 10 samples (2013-01, 46°32'51"S, 24°11"E; 2013-02, 46°33'21"S, 24°23"E) using the ID-TIMS method at the Institute of Geology and Mineral Resources, Chinese Academy of Geological Sciences (Wang et al., 2004). The analytical conditions are as follows: heating temperature, 1000°C; heating time, 1 min; heating rate, 10°C/min; cooling rate, 10°C/min; sample size, 100 µg; counting time, 1000 s; blank value, 1000 ppm; detection limit, 100 ppm. The analytical results are shown in Table 1. The concordia diagram shows that the samples are concordant, with an overall concordance of 95% (Fig. 1). The weighted mean age of the samples is 11.1 ± 0.2 Ma (n = 10, 95% confidence interval), which is consistent with the age of the samples (11.1 ± 0.2 Ma) obtained by the Rb-Sr method (Wang et al., 2011).

4. e 1. . . . , e

| | 2013 | 01-1 | 2013 | 01-3 | 2013 | 01-4 | 2013 | 01-5 | 2013 | 01-6 | 2013 | 01- | 2013 | 01- | 2013 | 01. 1 | 2013 | 01. 2 | 2013 | 01. 4 |
|----------------------|-------|-------|-------|-------|-------|------|-------|------|-------|------|-------|-----|-------|-------|-------|-------|-------|-------|-------|-------|
| | e | %e | e | %e | e | %e | e | %e | e | %e | e | %e | e | %e | e | %e | e | %e | e | %e |
| Major elements (%) | | | | | | | | | | | | | | | | | | | | |
| O | 0.005 | | 0.064 | | 0.00 | | 0.005 | | 0.00 | | 0.003 | | 0.003 | | 0.051 | | 0.044 | | 0.222 | |
| Si | 0.021 | | 0.34 | | 0.044 | | 0.042 | | 0.0 2 | | 0.031 | | 0.033 | | 0.310 | | 0.25 | | 1.450 | |
| Al | 0.004 | | 0.04 | | 0.00 | | 0.00 | | 0.011 | | 0.005 | | 0.005 | | 0.04 | | 0.043 | | 0.21 | |
| Mg | 0.011 | | 0.232 | | 0.036 | | 0.044 | | 0.012 | | 0.034 | | 0.00 | | 0.123 | | 0.0 0 | | 0. 3 | |
| Ca | 0.0 0 | | 0.036 | | 0.03 | | 0.03 | | 0.06 | | 0.026 | | 0.025 | | 0.046 | | 0.031 | | 0.06 | |
| Na | 0.26 | | 1. 10 | | 6.600 | | 1. 0 | | 0. 3 | | 0.233 | | 1.150 | | 1.5 0 | | 0.516 | | 0.1 5 | |
| K | 0.406 | | 0.0 2 | | 0.12 | | 0.112 | | 0.0 | | 0.1 | | 0.054 | | 0.16 | | 0.1 1 | | 0.6 5 | |
| Sc | 0.046 | | 0.034 | | 0.014 | | 0.02 | | 0.050 | | 0.030 | | 0.010 | | 0.050 | | 0.02 | | 0.130 | |
| Ti | 0.1 1 | | 0.144 | | 0.203 | | 0.364 | | 0.042 | | 0.0 4 | | 0.0 | | 0.066 | | 0.042 | | 0.0 3 | |
| Major elements (ppm) | | | | | | | | | | | | | | | | | | | | |
| O | 2013 | 01. 5 | 2013 | 01. 6 | 2013 | 01. | (1) | | 2013 | 01. | (1) | | 2013 | 03. 2 | (1) | | 2013 | 03. 3 | (1) | |
| Si | 0.34 | | 0.15 | | 1.40 | | 1.24 | | 1.31 | | 1. 0 | | 1.63 | | 1.31 | | 1.1 | | 0.33 | |
| Al | 1. . | | 1. 5 | | 16.5 | | 16.1 | | 15. 3 | | 15. | | 16. 6 | | 15.55 | | 15.4 | | 1. 61 | |
| Mg | 4.52 | | 3.34 | | .11 | | .43 | | .0 | | .13 | | .11 | | .42 | | .2 | | 3.44 | |
| Ca | 0.0 | | 0.0 | | 0.11 | | 0.10 | | 0.11 | | 0.13 | | 0.11 | | 0.14 | | 0.12 | | 0.0 | |
| Na | 6. | | .42 | | 4. 0 | | 4.2 | | 4.41 | | 5. | | 3.2 | | 6.06 | | .14 | | 4. | |
| Sc | 11.03 | | 12.61 | | 6.22 | | 5. 5 | | 6.3 | | 6. 5 | | 4.52 | | .4 | | .26 | | . 0 | |
| Ti | 4. 6 | | .3 | | .2 | | .3 | | .00 | | 4.52 | | .31 | | 4. 0 | | 4.0 | | .11 | |
| Sc | 0.13 | | 0.11 | | 0.3 | | 0.31 | | 0.42 | | 2.04 | | 0.33 | | 1.2 | | 2.03 | | 0.1 | |
| Sc | 0.04 | | 0.02 | | 0.62 | | 0.62 | | 0.65 | | 0. 4 | | 0.6 | | 0.4 | | 0.44 | | 0.04 | |
| Sc | 3. 2 | | 3.26 | | 4.24 | | 2.54 | | 2. 3 | | 2.2 | | 5.14 | | 2.65 | | 1. 3 | | 2. . | |
| Sc | 5 | | .2 | | .6 | | .0 | | .4 | | .40 | | .1 | | .6 | | .6 | | . 1 | |
| Sc | 4. | | .4 | | .11 | | .0 | | .42 | | 6.56 | | .64 | | 6.0 | | 6.11 | | .2 | |
| # | 5 | | 1 | | 55 | | 54 | | 54 | | 56 | | 41 | | 56 | | 64 | | 4 | |
| Trace elements (ppm) | | | | | | | | | | | | | | | | | | | | |
| Sc | 0.0 | | 4. 5 | | 1.16 | | 1.12 | | 1.4 | | .0 | | 40.4 | | 5.2 | | 6. 2 | | 5. 1 | |
| Sc | 0.22 | | 0.135 | | 1.2 4 | | 1.6 3 | | 1.316 | | 1. 53 | | 1.034 | | 1.100 | | 0.5 5 | | 0.62 | |
| Sc | 25.0 | | 23. | | 1. 6 | | 1. 5 | | 1. 5 | | .5 | | 1. 2 | | 25.2 | | 1 . | | 1. 0 | |
| Sc | 11 | | 3. | | 1 6 | | 166 | | 1. 2 | | 22 | | 22 | | 254 | | 1 | | 5. | |
| Sc | 34. | | 163 | | 60.5 | | 62.6 | | 64.1 | | 116 | | 1 . | | 0. | | 203 | | 23. | |
| Sc | 24.2 | | 21.6 | | 26. | | 23.6 | | 24.6 | | 2 . | | 2. 5 | | 2. 0 | | 2. 0 | | 16.4 | |
| Sc | 4. | | 1 5 | | 63.6 | | 50. | | 51.4 | | 6. | | 2 . | | 5. 3 | | 132 | | 1. 1 | |

Table 1.

| | 2013 | 01. 5 | 2013 | 01. 6 | 2013 | 01. (1) | 2013 | 01. (1) | 2013 | 01. (1) | 2013 | 03. 2 (1) | 2013 | 03. 3 (1) | 2013 | 03. 4 (1) | 2013 | 03. 5 (1) | 2013 | 01. 3 (2) |
|-----|------|-------|------|-------|-------|---------|-------|---------|-------|---------|-------|-----------|-------|-----------|-------|-----------|-------|-----------|------|-----------|
| %de | 3. | | 1.20 | | 3 .60 | (1) | 46. 0 | (1) | 4 .30 | (1) | 23.40 | (1) | 43.00 | (1) | 25.20 | (1) | 32. 0 | (1) | 6.56 | |

Table 1.

| | 2013 (%) | 01. 11 (2) | 2013 (%) | 02. 1 (2) | 2013 (%) | 02. 2 (2) | 2013 (%) | 03. 1 (1) | 2013 (%) | 03. 6 (1) | 2013 (%) | 01. 10 (2) | 04. 06 (1) | 04. 24 (1) | 04. 2 (1) | 03. 1 (1) |
|----------------------|-------------|---------------|-------------|--------------|-------------|--------------|-------------|--------------|-------------|--------------|-------------|---------------|---------------|---------------|--------------|--------------|
| Trace elements (ppm) | | | | | | | | | | | | | | | | |
| Al | 1.4 | 36. | 42.4 | 26.0 | 32.4 | 1. | / | / | / | / | / | / | / | / | / | / |
| B | 0.35 | 0.153 | 0.35 | 1.1 | 0.4 | 0.46 | / | / | / | / | / | / | / | / | / | / |
| Ce | 32.5 | 33.2 | 34.5 | 25.1 | 26.3 | 32.1 | 13.4 | 20.5 | 1. | 20.3 | | | | | | |
| Eu | 1.4 | 203 | 21 | 33 | 341 | 1.5 | 144 | 14 | 214 | 265 | | | | | | |
| Ga | 56.5 | 44.2 | 4. | 1. | 22.2 | 53. | 15 | 162 | 214 | 265 | | | | | | |
| Hf | 34. | 3.5 | 3.3 | 23.1 | 24. | 33. | 20.6 | 30. | 2. | 20.2 | | | | | | |
| K | 66.4 | 4.6 | 6.4 | 25.4 | 2.1 | 66.6 | .1 | 114 | 5.5 | .02 | | | | | | |
| La | 6.4 | 236.4 | 256. | 205.4 | 20. | 114.20 | / | / | / | / | | | | | | |
| Mg | 4.0 | 44.1 | 4.0 | 4. | 103 | 44.1 | / | / | / | / | | | | | | |
| Nd | 12.0 | 11.1 | 11.2 | 14. | 13.6 | 12.0 | / | / | / | / | | | | | | |
| Pr | 0.5 | 1.420 | 1.00 | 3.130 | 3.20 | 0.53 | 4. | 1.1 | 22.0 | 1.2 | | | | | | |
| Rb | 1 | 1.50 | 5 | 20 | 24 | 66 | 1 | 31 | 111 | 6 | | | | | | |
| Sr | 13.0 | 13.0 | 13.2 | 21.1 | 22. | 12.5 | 13.2 | 13.2 | 14. | 20.1 | | | | | | |
| Ta | 54. | 42.3 | 41.5 | 144 | 154 | 52. | 243 | 133 | 164 | 151 | | | | | | |
| Tb | 1.2 | 0.4 | 0.55 | 11.315 | 11.5 | 1.25 | 20.2 | 12. | 21. | 12.2 | | | | | | |
| Tb | 0.025 | 0.030 | 0.02 | 0.051 | 0.052 | 0.02 | / | / | / | / | | | | | | |
| Tm | 0.31 | 0.26 | 0.32 | 1.560 | 1.450 | 0.360 | / | / | / | / | | | | | | |
| Tb | 0.2 | 1.20 | 1.030 | 0.365 | 0.406 | 0.336 | / | / | / | / | | | | | | |
| Tb | 11 | 32 | 346 | 25 | 50 | 4.3 | / | / | / | / | | | | | | |
| Tb | 10.0 | .40 | .610 | 26.40 | 26.0 | 10.50 | 30.6 | 32.2 | 40.1 | 26.4 | | | | | | |
| Tb | 23.00 | 1.0 | 1.40 | 51.50 | 54.0 | 22.30 | 5. | 62. | 2.3 | 52.5 | | | | | | |
| Tb | 2.0 | 2.520 | 2.510 | 5.50 | 6.10 | 2.60 | 6. | .4 | 10.5 | 6.4 | | | | | | |
| Tb | 11.0 | 11.0 | 11.60 | 22.30 | 24.30 | 11.60 | 2.5 | 31.2 | 43.1 | 24.4 | | | | | | |
| Tb | 2.540 | 2.00 | 2.60 | 4.40 | 4.00 | 2.30 | 4.5 | 5.2 | 6. | 4.5 | | | | | | |
| Tb | 0.6 | 0.1 | 0.0 | 1.163 | 1.25 | 0.3 | 1.45 | 1.5 | 2.0 | 1.03 | | | | | | |
| Tb | 2.40 | 2.13 | 2.54 | 4.14 | 4.46 | 2.522 | 3.56 | 4.01 | 5.35 | 4.23 | | | | | | |
| Tb | 0.36 | 0.3 | 0.3 | 0.612 | 0.660 | 0.34 | 0.4 | 0.54 | 0.64 | 0.63 | | | | | | |
| Tb | 2.10 | 2.150 | 2.220 | 3.420 | 3.60 | 2.130 | 2.5 | 2. | 3.24 | 3.5 | | | | | | |
| Tb | 0.46 | 0.446 | 0.444 | 0.2 | 0.5 | 0.46 | 0.4 | 0.52 | 0.5 | 0. | | | | | | |
| Tb | 1.350 | 1.230 | 1.240 | 2.120 | 2.20 | 1.310 | 1.32 | 1.3 | 1.45 | 2.25 | | | | | | |
| Tb | 0.10 | 0.16 | 0.15 | 0.304 | 0.32 | 0.14 | 0.1 | 0.2 | 0.2 | 0.34 | | | | | | |
| Tb | 1.210 | 1.050 | 1.120 | 1.60 | 2.110 | 1.210 | 1.25 | 1.23 | 1.24 | 2.13 | | | | | | |
| Tb | 0.14 | 0.164 | 0.165 | 0.21 | 0.323 | 0.13 | 0.20 | 0.1 | 0.1 | 0.34 | | | | | | |
| Tb | 1.30 | 0.41 | 1.040 | 3.20 | 3.510 | 1.460 | 5.3 | 3.2 | 4.16 | 3.2 | | | | | | |
| Tb | 0.04 | 0.062 | 0.051 | 0.5 | 0.644 | 0.0 | 1.35 | 0.6 | 1.16 | 0.6 | | | | | | |
| Tb | 0.151 | 2.0 | 1.50 | 2.5 | 1. | 0.33 | / | / | / | / | | | | | | |
| Tb | 0.34 | 0.206 | 0.200 | 45.20 | 35.10 | 0.41 | .13 | .0 | 4.1 | 21.06 | | | | | | |
| Tb | 1.0 | 0.61 | 0.1 | .60 | .20 | 1.0 | 4.50 | 2.63 | 3.20 | .41 | | | | | | |
| Tb | 0.500 | 0.304 | 0.302 | 2.30 | 3.40 | 0.501 | 1. | 0.6 | 1.46 | 2.5 | | | | | | |

Table 1. Trace elements (ppm) of the samples used in this study. Data are taken from [Bhattacharya et al. \(2009a\)](#).

$\epsilon_{\text{Nd}}(t) = 10000((^{143}\text{Nd}/^{144}\text{Nd})_0(t)/(^{143}\text{Nd}/^{144}\text{Nd})_0 - 1) + \epsilon_{\text{Nd}}(0) + (1/\sigma_{\text{Nd}}^2)^{1/2}$

| | | ϵ_{Nd} | (1 σ) | |
|------|--------|------------------------|---------------|------------------------|---------------|------------------------|---------------|------------------------|---------------|------------------------|---------------|------------------------|---------------|------------------------|---------------|------|
| 2013 | 01. 3 | -4.2 | (2) | 0.36 | 3.2 | 0.002 | 0.04030(2) | 0.04015 | 2.4 | 10. | 0.13 | 4 | 0.512 | 3. (40) | 0.5124 | 4.6. |
| 2013 | 01. 10 | -4.2 | (2) | 0.5 | 6.6 | 0.0024 | 0.045 (23) | 0.0445 | 2.3 | 11.6 | 0.1235 | 0.512 | 0. (43) | 0.5124 | 6.1 | |
| 2013 | 03. 1 | -4.1 | (1) | 3.13 | 2.0 | 0.0335 | 0.06324(20) | 0.06133 | 4.4 | 22.3 | 0.121 | 0.512533(4) | 0.512214 | 1. | | |
| 2013 | 03. 2 | -4.1 | (1) | 2. | 1320 | 0.0063 | 0.042 (20) | 0.04255 | 4.5 | 2.6 | 0.1046 | 0.512 | 1. (51) | 0.512445 | 6.3 | |
| 2013 | 03. 3 | -4.1 | (1) | .06 | 516 | 0.0452 | 0.0536 (43) | 0.05111 | 5. | 36. | 0.0 | 0.512 | 0. (30) | 0.512450 | 6.4 | |
| 2013 | 03. 4 | -4.1 | (1) | .65 | 14.0 | 0.01 | 0.0422 (51) | 0.04120 | 4.55 | 24.5 | 0.1123 | 0.512 | 03(53) | 0.51250 | .5 | |

$$\epsilon_{\text{Nd}}(t) = 10000((^{143}\text{Nd}/^{144}\text{Nd})_0(t)/(^{143}\text{Nd}/^{144}\text{Nd})_0 - 1) + \epsilon_{\text{Nd}}(0) + (1/\sigma_{\text{Nd}}^2)^{1/2}$$

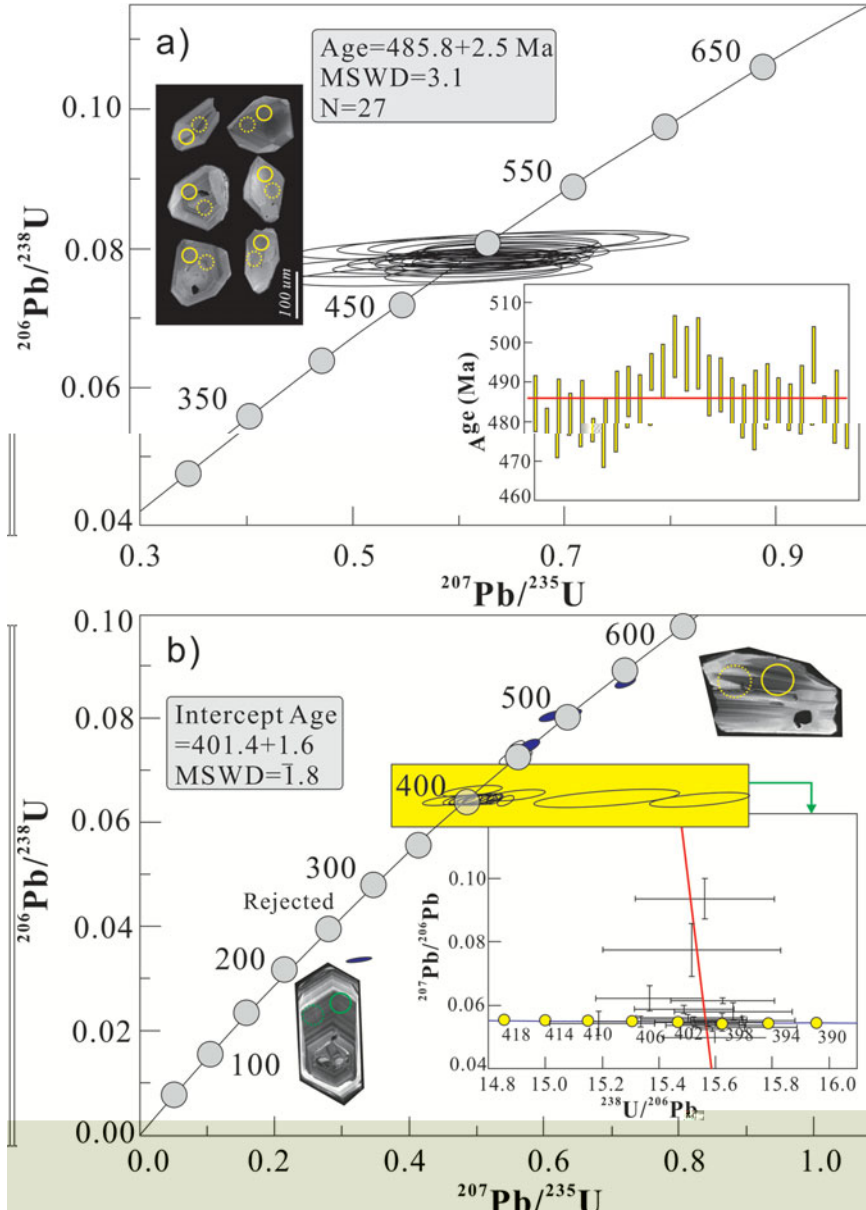


Fig. 4. (a) Concordia plot of $^{206}\text{Pb}/^{238}\text{U}$ vs. $^{207}\text{Pb}/^{235}\text{U}$ for zircon. (b) Concordia plot of $^{206}\text{Pb}/^{238}\text{U}$ vs. $^{207}\text{Pb}/^{235}\text{U}$ for zircon. Error bars represent 1 σ uncertainties. $\pm 1\sigma$ error ellipses are shown for each point. $\pm 2\sigma$ error ellipses are shown for the intercepts.

($\pm 4\%$, $n = 2$, $R = 3.1$). The ϵ_{Nd} values ($\pm 1\sigma$, $\pm 1\sigma$) are -4.2 ± 4.4 and -4.1 ± 4.4 (Table 1; Fig. 4), which are $\sim 1\%$ lower than the values of -3.1 ± 4.4 and -3.0 ± 4.4 reported by Li et al. (2003). The ϵ_{Nd} values ($\pm 1\sigma$, $\pm 1\sigma$) are -4.1 ± 4.4 and -3.0 ± 4.4 (Table 1; Fig. 4), which are $\sim 1\%$ lower than the values of -3.1 ± 4.4 and -3.0 ± 4.4 reported by Li et al. (2003). The ϵ_{Nd} values ($\pm 1\sigma$, $\pm 1\sigma$) are -4.1 ± 4.4 and -3.0 ± 4.4 (Table 1; Fig. 4), which are $\sim 1\%$ lower than the values of -3.1 ± 4.4 and -3.0 ± 4.4 reported by Li et al. (2003).

e % . . . , e e e e e %
 e ee (2, ee e . 4).
 e % ee % e e e e e
 e .. e 1 e e e e 1 e 2
 e % e e e e e 450
 500. e e e % e e e % e e
 21 e % e 1 e e e 1 e % e e
 e 206 23 e e e e e e
 401 ± 2 (= 3.3) e e e e
 e ee 206 23 e e 20 235 e e e e
 e e e e e e e % e e e
 e ee 1 e 401.4 ± 1.6 (= 1.) (ee
 e . . . 4), e e e e e e 206
 23 e e e e e e e e e e
 e e e e e e e e e e 1 3).

4.b. M a c

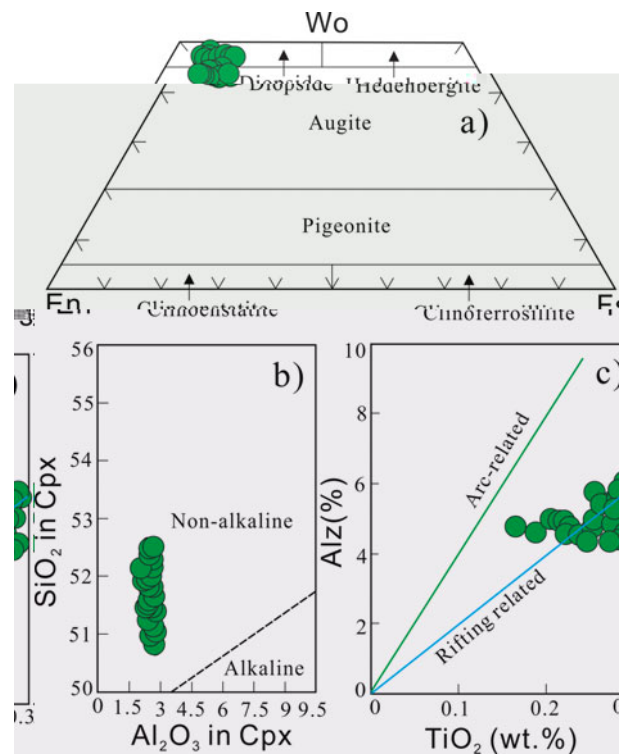
4.b.1. Spinel composition

4.b.2. Pyroxene compositions

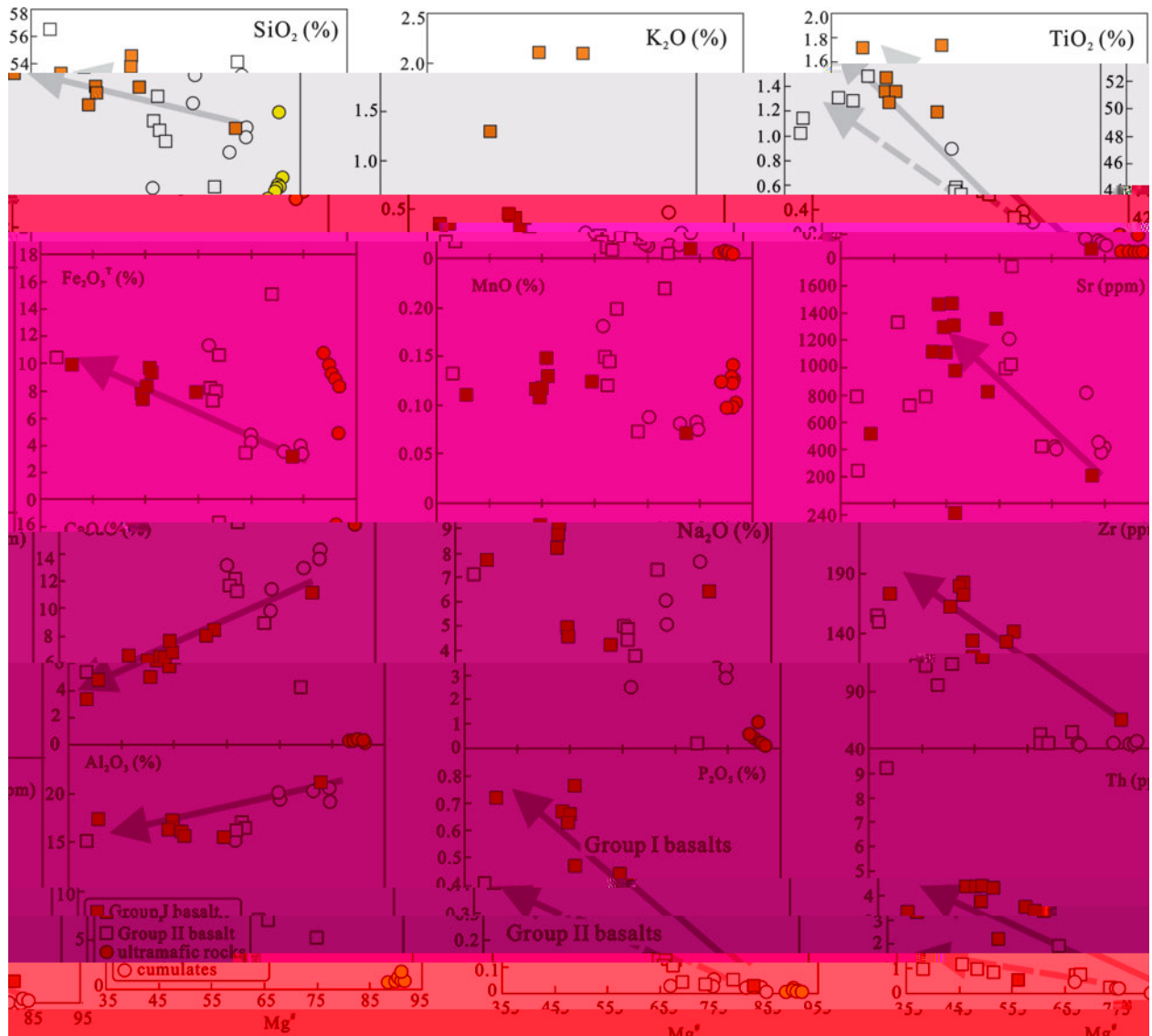
4.c. W - c a c

4.c.1. Serpentinites and cumulates

(> 12%, 40%), (1.0%), (0.03–0.06%), (0.04–0.2%) (0.04–0.05%).



e 5. () e ()
e 1. e 1% e e
(e 1. e () . 2 (%) . 2 3 (%) (2)
(e e e e e e e 1 e %) . 2 (%)
e 1% e e e e e 1 e e



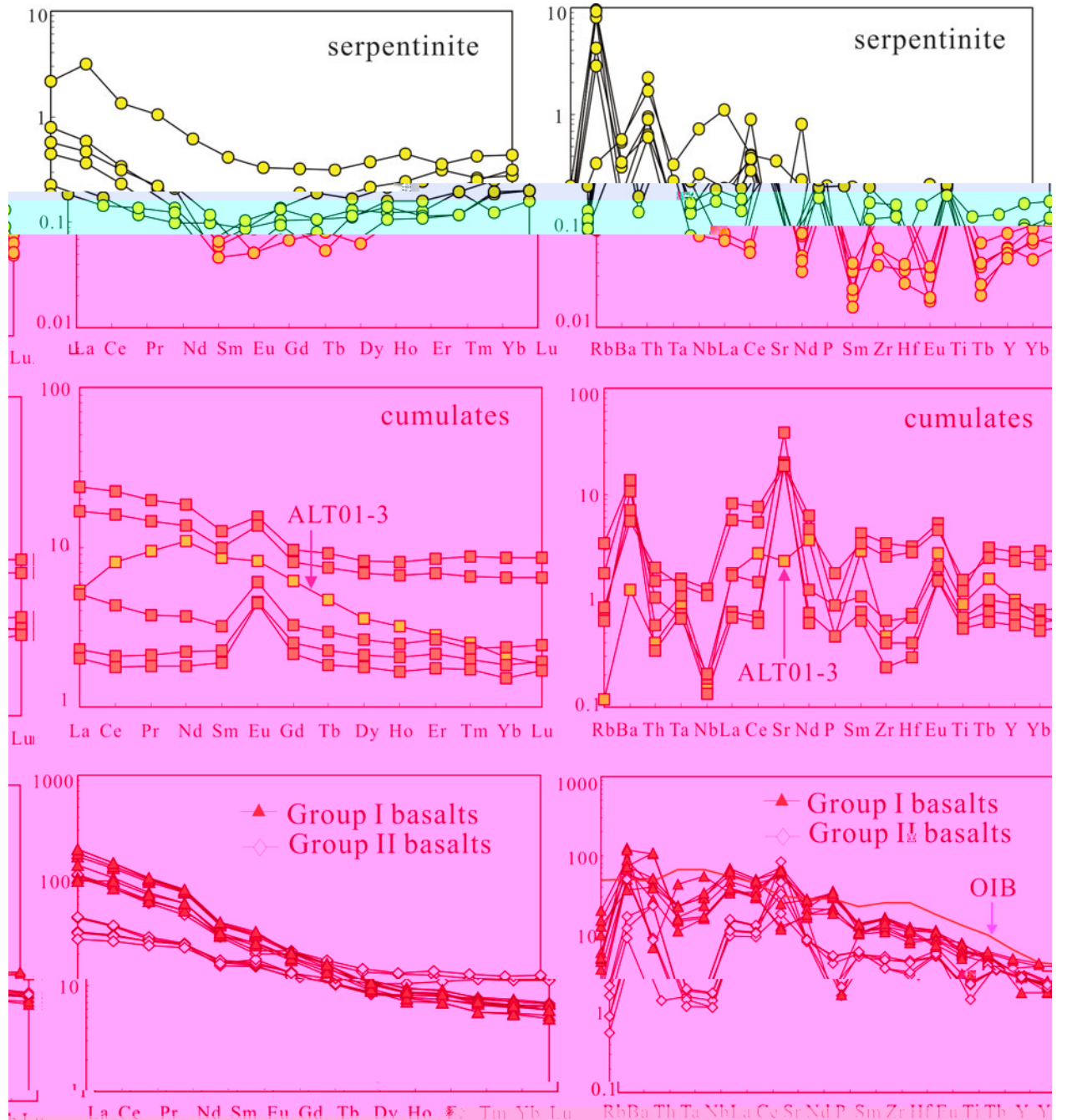


Fig. 1. REE patterns of serpentinites, cumulates and basalts. The patterns are plotted on a logarithmic scale. The patterns of serpentinites and cumulates are similar to those of the OIB (Olivine-rich Intraplate Basalts) (14).

the REE patterns of Group I basalts ($\text{Ce}/\text{La} = 0.0-1.14$) (15). The Ce/La ($\text{Ce}/\text{La} = 1.02-1.21$) (16) and Ce/La ($\text{Ce}/\text{La} = 1.44-1.64$) ($\text{Ce}/\text{La} = 0.44$) (17) basalts have similar REE patterns. The REE patterns of Group II basalts ($\text{Ce}/\text{La} = 0.11$) (18) are similar to those of the basalts ($\text{Ce}/\text{La} = 0.11$) (19).

W-S-Na-zg-H-O ($\text{Ce}/\text{La} = 1.02-1.21$) (20) ($\text{Ce}/\text{La} = 1.02-1.21$) (21) ($\text{Ce}/\text{La} = 0.0024-0.0452$) ($\text{Ce}/\text{La} = 0.04030-0.0536$) (22) ($\text{Ce}/\text{La} = 0.04015-0.05111$) (23) (2013-03-1) ($\text{Ce}/\text{La} = 0.13-4$) (24) ($\text{Ce}/\text{La} = 0.0-0.13-4$) (25) ($\text{Ce}/\text{La} = 0.512-0.512-3$) ($\text{Ce}/\text{La} = 0.512-0.512-3$) (26) ($\text{Ce}/\text{La} = +6.3-+5.5$) (2013-03-1) ($\text{Ce}/\text{La} = +1$).

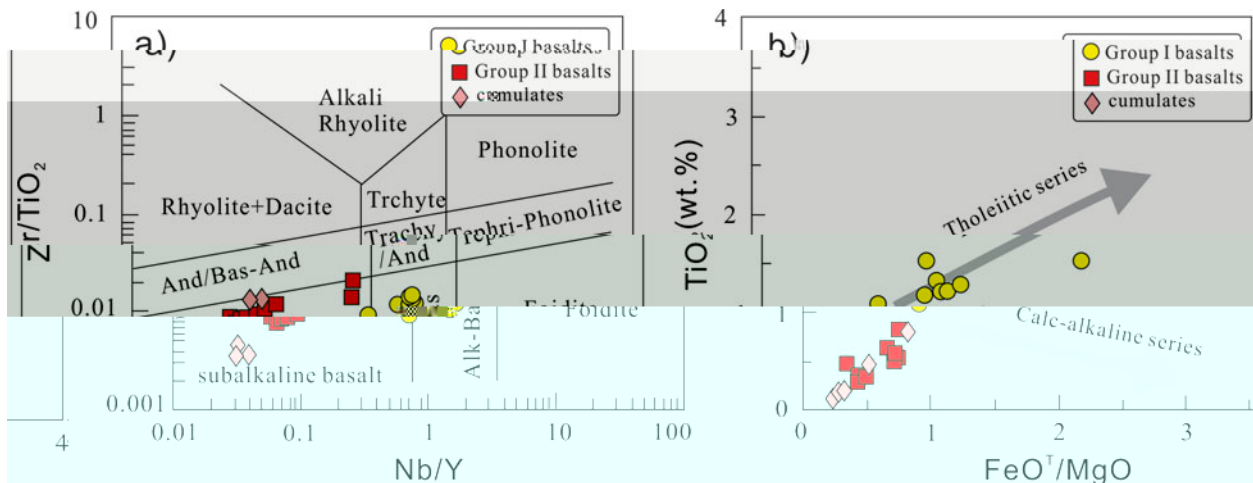


Fig. 2. (a) Zr/TiO₂ vs. Nb/Y and (b) TiO₂ (wt. %) vs. FeO^T/MgO. The field boundaries are after Le Maitre et al. (1989). The Tholeiitic series and Calc-alkaline series are after Le Maitre & Taylor (1991). The data points are the same as in Fig. 1.

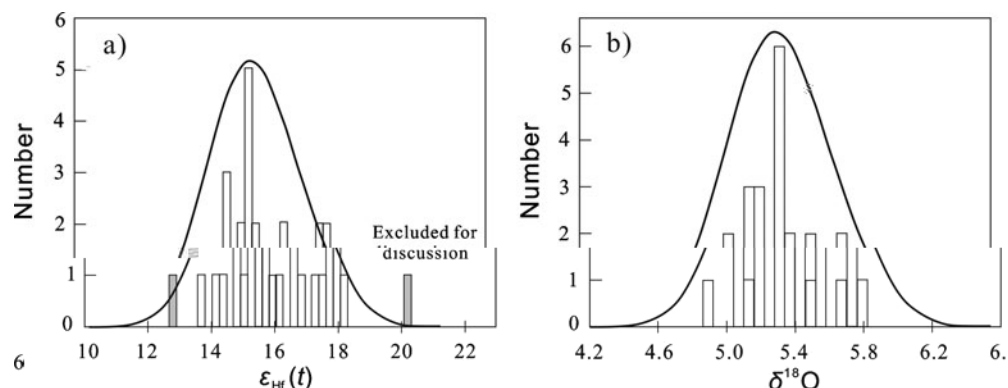


Fig. 3. (a) Distribution of ε_{Hf}(t) and (b) δ¹⁸O.

ε_{Hf}(t) = 14.1 ± 1.1 (n = 11, 1e-01%), ε_{Hf}(t) = 14.2 ± 1.1 (n = 11, 1e-01%), ε_{Hf}(t) = 14.5 ± 1.1 (n = 13, 2.0%), ε_{Hf}(t) = 15.5 ± 1.5 (n = 1, 1e-01%), ε_{Hf}(t) > 16.0 (n = 1, 1e-01%), ε_{Hf}(t) < 12.0 (n = 1, 1e-01%), ε_{Hf}(t) < 13.0 (n = 1, 1e-01%), ε_{Hf}(t) < 14.0 (n = 1, 1e-01%), ε_{Hf}(t) < 15.0 (n = 1, 1e-01%), ε_{Hf}(t) < 16.0 (n = 1, 1e-01%), ε_{Hf}(t) < 17.0 (n = 1, 1e-01%), ε_{Hf}(t) < 18.0 (n = 1, 1e-01%), ε_{Hf}(t) < 19.0 (n = 1, 1e-01%), ε_{Hf}(t) < 20.0 (n = 1, 1e-01%), ε_{Hf}(t) < 21.0 (n = 1, 1e-01%).

δ¹⁸O = ~400 (n = 1, 1e-01%), ε_{Hf}(t) = 14.1 ± 1.4 (n = 2, 1e-01%), ε_{Hf}(t) = 16.0 ± 2.0 (n = 1, 1e-01%), ε_{Hf}(t) = 17.0 ± 1.0 (n = 1, 1e-01%), ε_{Hf}(t) = 18.0 ± 1.0 (n = 1, 1e-01%) (Li et al. 2000).

5. Discussion

5.a. Tectonic setting of Zhaheba

The tectonic setting of the Zhaheba ophiolite is discussed based on the petrology and geochemistry of the basalts. The basalts have a wide range of compositions, from subalkaline to alkali-rich, and show a clear differentiation trend from tholeiitic to calc-alkaline. The ε_{Hf}(t) values are mostly between 14 and 16, with one outlier at ~18. The δ¹⁸O values range from ~4.5 to 5.5‰. The trace element patterns show a clear differentiation trend from subalkaline to alkali-rich, with increasing Zr, Ti, and REE concentrations and decreasing Ni, Cr, and V. The REE patterns are generally flat to slightly LREE-enriched. The Sr and Nd isotopes show a clear differentiation trend from subalkaline to alkali-rich, with increasing ε_{Nd} and decreasing ε_{Sr}. The ε_{Nd} values range from ~-10 to +10, and the ε_{Sr} values range from ~-10 to +10. The Hf isotopes are relatively uniform, with ε_{Hf}(t) values ranging from ~-10 to +10. The O isotopes are relatively uniform, with δ¹⁸O values ranging from ~4.5 to 5.5‰. The trace element patterns and isotopic data suggest that the basalts were derived from a single source, likely a mantle plume, and underwent fractional crystallization and magma mixing during their ascent through the crust.

The tectonic setting of the Zhaheba ophiolite is discussed based on the petrology and geochemistry of the basalts. The basalts have a wide range of compositions, from subalkaline to alkali-rich, and show a clear differentiation trend from tholeiitic to calc-alkaline. The ε_{Hf}(t) values are mostly between 14 and 16, with one outlier at ~18. The δ¹⁸O values range from ~4.5 to 5.5‰. The trace element patterns show a clear differentiation trend from subalkaline to alkali-rich, with increasing Zr, Ti, and REE concentrations and decreasing Ni, Cr, and V. The REE patterns are generally flat to slightly LREE-enriched. The Sr and Nd isotopes show a clear differentiation trend from subalkaline to alkali-rich, with increasing ε_{Nd} and decreasing ε_{Sr}. The ε_{Nd} values range from ~-10 to +10, and the ε_{Sr} values range from ~-10 to +10. The Hf isotopes are relatively uniform, with ε_{Hf}(t) values ranging from ~-10 to +10. The O isotopes are relatively uniform, with δ¹⁸O values ranging from ~4.5 to 5.5‰. The trace element patterns and isotopic data suggest that the basalts were derived from a single source, likely a mantle plume, and underwent fractional crystallization and magma mixing during their ascent through the crust.

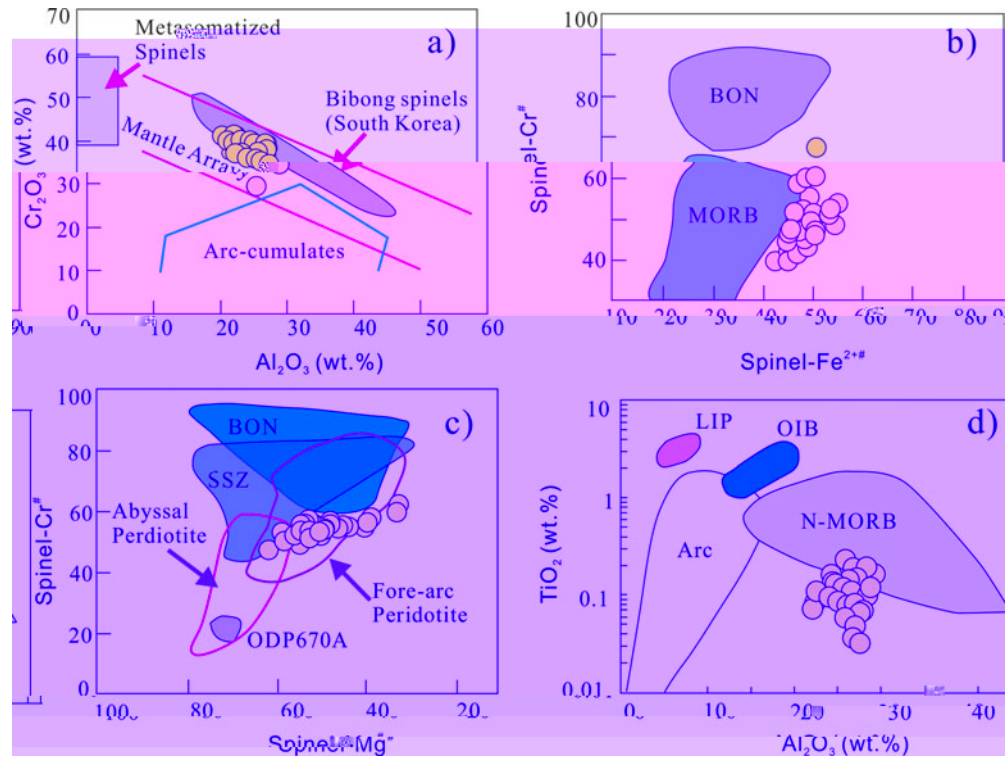
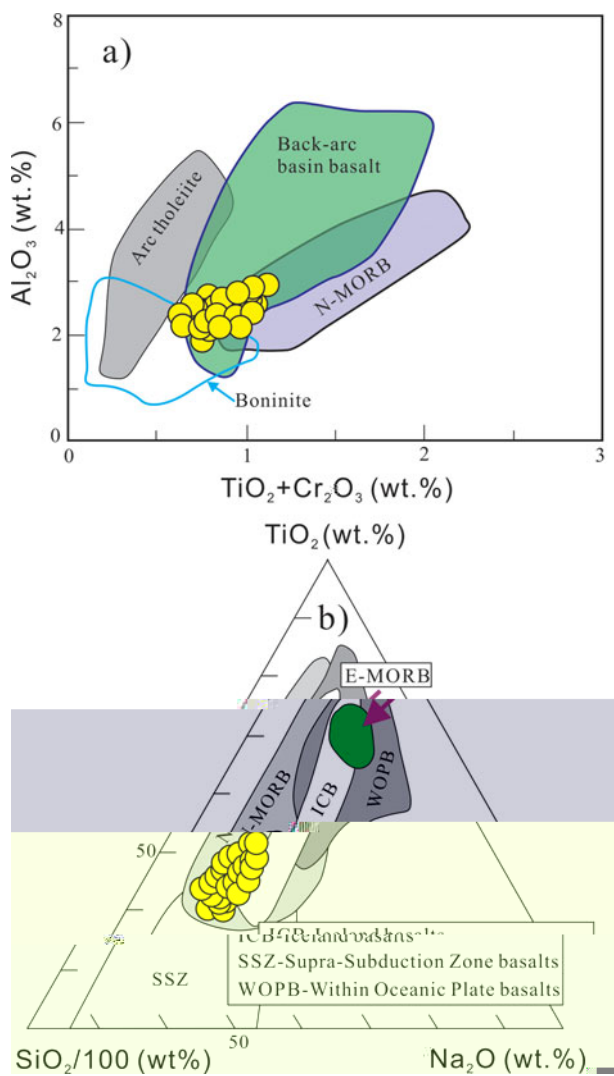


Fig. 10. (a) Cr_2O_3 vs Al_2O_3 (wt.%) (modified from & , 2000). (b) Spinel-Cr^* vs Spinel-Fe^{2+*} (modified from & , 2001). (c) Spinel-Cr^* vs Spinel-Mg^* (modified from & et al., 1995). (d) TiO_2 (wt.%) vs Al_2O_3 (wt.%) (modified from & , 2001). The shaded areas represent the ranges of spinel compositions in mantle arrays and arc-cumulates (modified from & , 2000).

(500–4000 ppm) (& et al. 2003, & et al. 2015), 1–10% (430–4000 ppm) (& et al. 2000b, 2014) and 1–10% (30–350 ppm) (& et al. 2003, & et al. 2006).

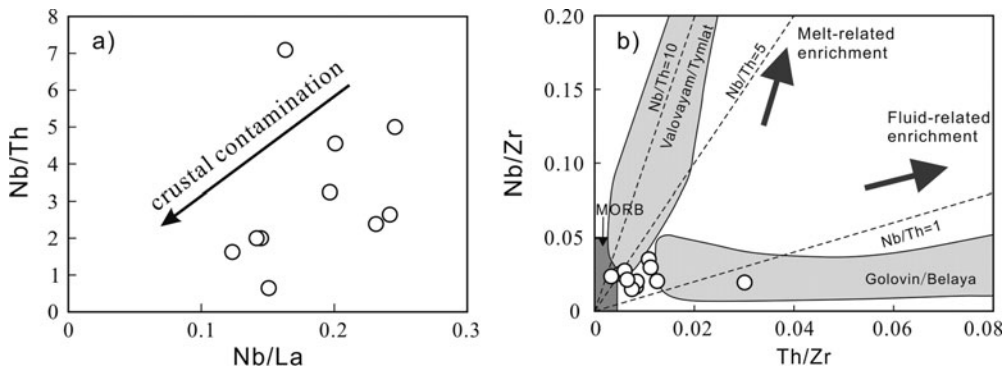
5.b. Olivine / spinel + a-cpx + pl

1–10% (1–1000 ppm) (& et al. 2002, & et al. 2010).

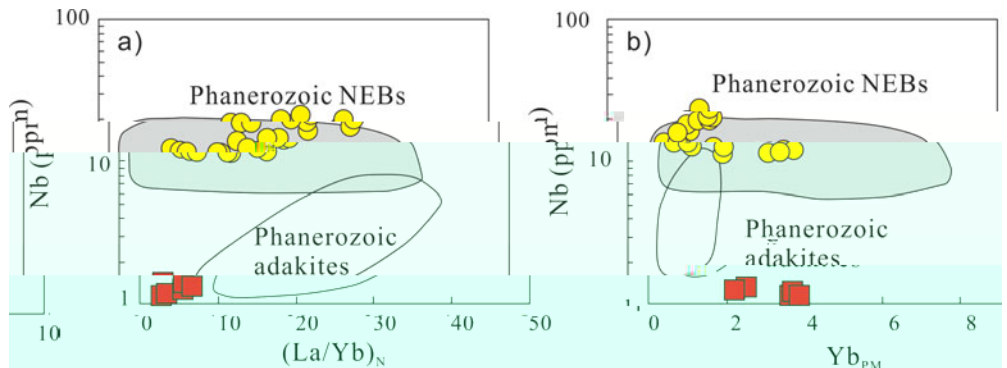


5.c. P D a ba

ee e e ee e % e e e e e
 e 1, e e 1 e e e e e
 e 2. 1 e e e e e (11 24 11,
 e 15 11), 2 5 (0.4 0.6%)
 (11 15, e 1 60) e e (e /)
 (e, e, e e e% e - e e e
 () (e e, e & , 1 2 -
 & e e, 2001) (13). e e e e
 ee e ee 1 1 e ee e e e
 e e e e e e e e e (1)
 e e e e e e e e 1 e ee
 e e e e e(e. . e & -
 %, 2002) (2) e e e e e e e
 e e % e (e e, e & ,
 1 2 e & , 1 3 e et al. 1 6).
 e e e ee e % e % e 1 e e
 e 1 e e e e 1 e e e



12. (6) / . / . / () e e, () e, () . () 1, . / . / () e e,
e, () e, () e, () 1, . e.



5. . I ca Pa a z c acc e

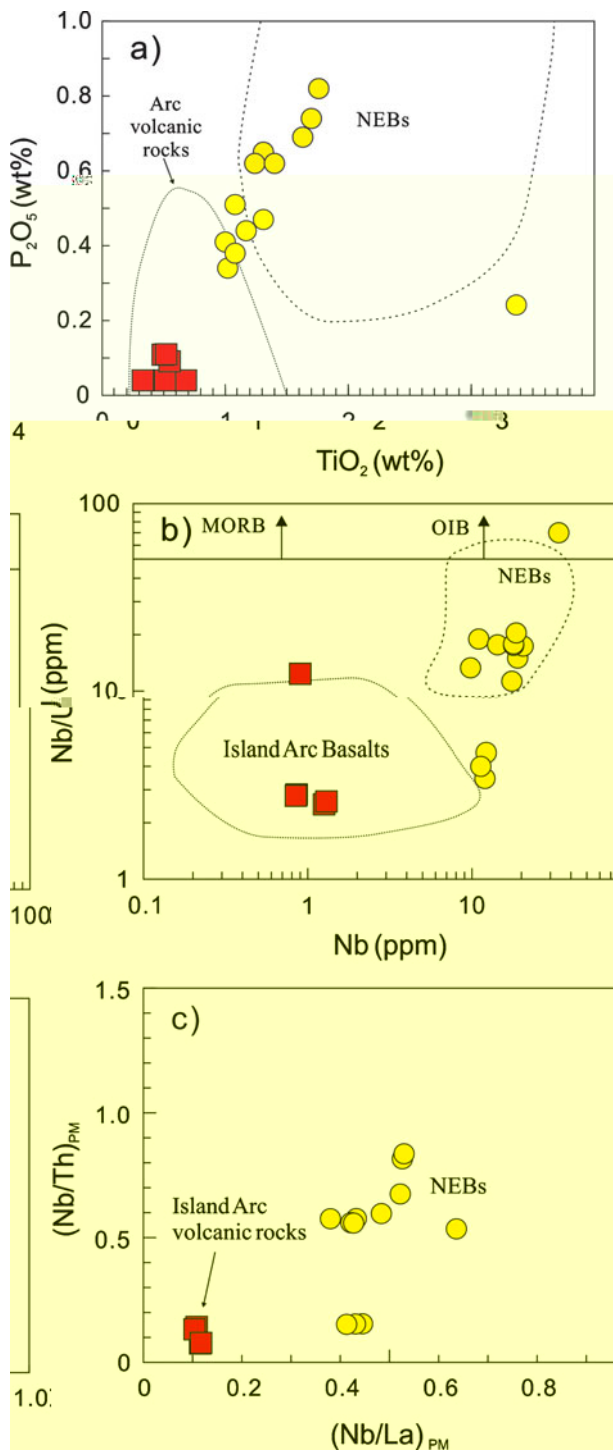


Fig. 14. (a) P_{2O_5} vs TiO_2 ; (b) Nb/U vs Nb ; (c) $(Nb/Th)_{PM}$ vs $(Nb/La)_{PM}$. NEBs, NEB basalts; Arc volcanic rocks, arc volcanic rocks. Data sources: NEBs (this study); Arc volcanic rocks (Xia et al. 2015).

NEBs have higher P_{2O_5} and lower TiO_2 than arc volcanic rocks (Fig. 14a), which is consistent with the higher P_{2O_5} and lower TiO_2 in NEBs (Table 2).

NEBs have higher Nb/U and lower Nb than island arc basalts (Fig. 14b), which is consistent with the higher Nb/U and lower Nb in NEBs (Table 2).

NEBs have higher $(Nb/Th)_{PM}$ and lower $(Nb/La)_{PM}$ than island arc volcanic rocks (Fig. 14c), which is consistent with the higher $(Nb/Th)_{PM}$ and lower $(Nb/La)_{PM}$ in NEBs (Table 2).

NEBs have higher P_{2O_5} and lower TiO_2 , Nb/U and higher $(Nb/Th)_{PM}$ than island arc volcanic rocks (Fig. 14a–c), which is consistent with the higher P_{2O_5} and lower TiO_2 , Nb/U and higher $(Nb/Th)_{PM}$ in NEBs (Table 2).

NEBs have higher P_{2O_5} and lower TiO_2 , Nb/U and higher $(Nb/Th)_{PM}$ than island arc basalts (Fig. 14a–c), which is consistent with the higher P_{2O_5} and lower TiO_2 , Nb/U and higher $(Nb/Th)_{PM}$ in NEBs (Table 2).

NEBs have higher P_{2O_5} and lower TiO_2 , Nb/U and higher $(Nb/Th)_{PM}$ than island arc volcanic rocks (Fig. 14a–c), which is consistent with the higher P_{2O_5} and lower TiO_2 , Nb/U and higher $(Nb/Th)_{PM}$ in NEBs (Table 2).

(1) NEBs have higher P_{2O_5} and lower TiO_2 than island arc basalts (Fig. 14a), which is consistent with the higher P_{2O_5} and lower TiO_2 in NEBs (Table 2).

(2) NEBs have higher Nb/U and lower Nb than island arc basalts (Fig. 14b), which is consistent with the higher Nb/U and lower Nb in NEBs (Table 2).

(3) NEBs have higher $(Nb/Th)_{PM}$ and lower $(Nb/La)_{PM}$ than island arc basalts (Fig. 14c), which is consistent with the higher $(Nb/Th)_{PM}$ and lower $(Nb/La)_{PM}$ in NEBs (Table 2).

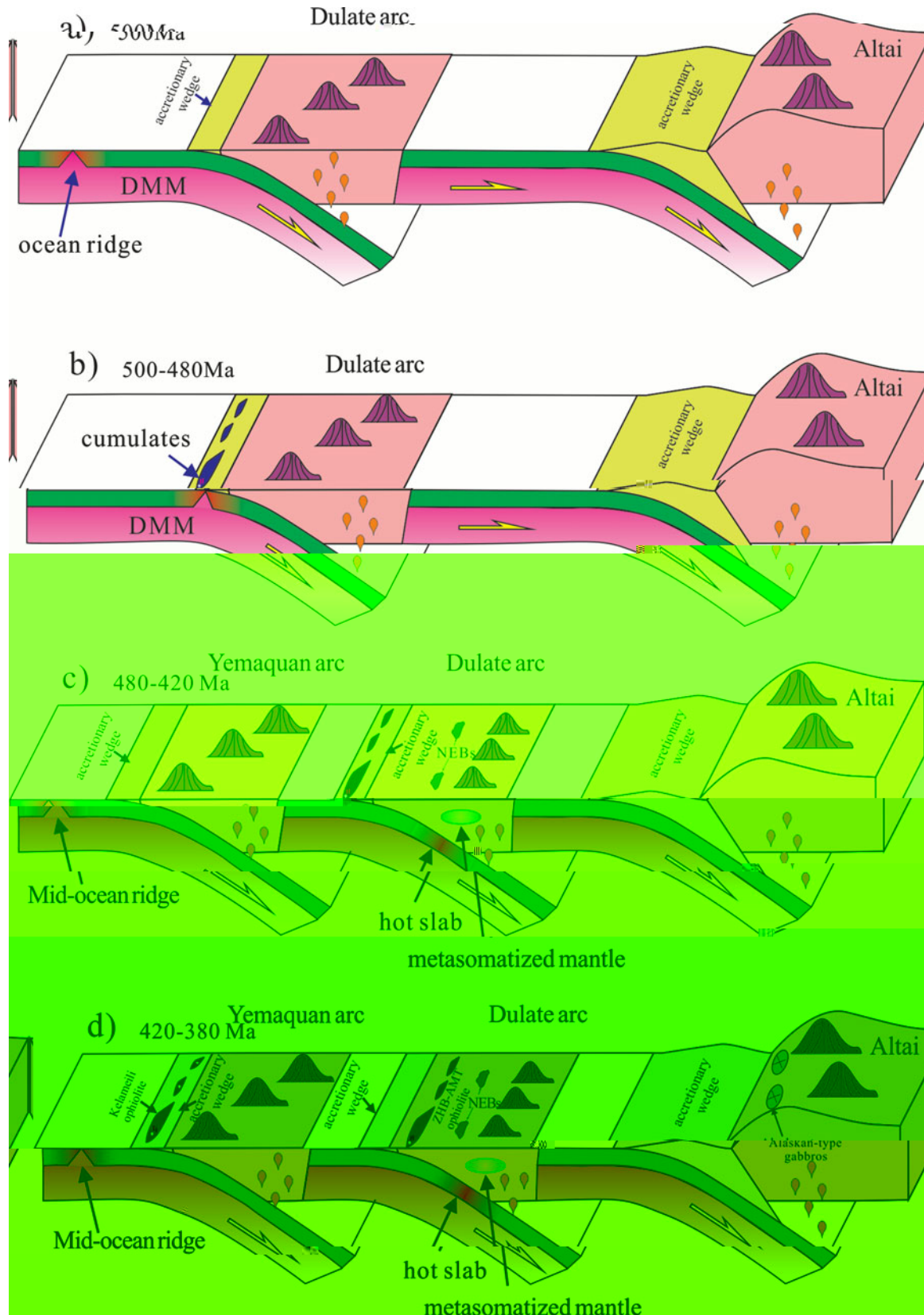


Figure 15. (a-d) Evolution of the Dulate arc and Yemaquan arc from ~590 Ma to 380 Ma. The Yemaquan arc is shown in green, and the Dulate arc is shown in yellow. The Altai region is to the east. NEBs = nepheline-rich plutons. Modified after Figure 1 of Li et al. (2016).

(4) $\text{Mg}^{2+}/(\text{Mg}^{2+} + \text{Fe}^{2+})$ (420 3.0.4) (Li et al. 2014; Li et al. 2015). The $\text{Mg}^{2+}/(\text{Mg}^{2+} + \text{Fe}^{2+})$ values range from 0.42 to 0.48, and the $\text{Mg}^{2+}/(\text{Mg}^{2+} + \text{Fe}^{2+})\%$ values range from 40.0% to 48.0%. The $\text{Mg}^{2+}/(\text{Mg}^{2+} + \text{Fe}^{2+})$ and $\text{Mg}^{2+}/(\text{Mg}^{2+} + \text{Fe}^{2+})\%$ values are 0.45–0.47 and 42.0–46.0%, respectively.

6. Conclusion

(1) The Zhaheba ophiolite is c. 45 Ma old, and the age is c. 400 Ma. The $\text{Mg}^{2+}/(\text{Mg}^{2+} + \text{Fe}^{2+})$ and $\text{Mg}^{2+}/(\text{Mg}^{2+} + \text{Fe}^{2+})\%$ values are 0.45–0.47 and 42.0–46.0%, respectively.

(2) The Zhaheba ophiolite is c. 1.0 Ga old, and the age is c. 1.0 Ga. The $\text{Mg}^{2+}/(\text{Mg}^{2+} + \text{Fe}^{2+})$ and $\text{Mg}^{2+}/(\text{Mg}^{2+} + \text{Fe}^{2+})\%$ values are 0.45–0.47 and 42.0–46.0%, respectively.

(3) The Zhaheba ophiolite is c. 1.0 Ga old, and the age is c. 1.0 Ga. The $\text{Mg}^{2+}/(\text{Mg}^{2+} + \text{Fe}^{2+})$ and $\text{Mg}^{2+}/(\text{Mg}^{2+} + \text{Fe}^{2+})\%$ values are 0.45–0.47 and 42.0–46.0%, respectively.

Ac
Author's biography:
Xiaoming Li obtained his Ph.D. in geological engineering from the China University of Geosciences (Beijing) in 2011 (06-03-01).

S7 a a a

Received 11 February 2016; accepted 10 May 2016; first published online 1 July 2016; DOI: 10.1017/geo.2016.56; available online 16 June 2016.

References

- Aliberti, L., 1994. The evolution of the Earth's crust: a review. *Chemical Geology* **113**, 1–112.
- Aliberti, L., & Sartori, M., 2001. The evolution of the Earth's crust: a review. *Journal of Petrology* **42**, 221–302.
- Aliberti, L., & Sartori, M., 2002. The evolution of the Earth's crust: a review. *Lithos* **97**, 2–11.
- Aliberti, L., & Sartori, M., 2002. The evolution of the Earth's crust: a review. *Geology* **30**, 9–10.
- Aliberti, L., & Sartori, M., 2002. The evolution of the Earth's crust: a review. *Earth Accretionary Systems in Space and Time* (ed. L. Aliberti & M. Sartori), 11, 1–36.
- Aliberti, L., & Sartori, M., 2002. The evolution of the Earth's crust: a review. *Geological Magazine* **139**, 1–13.
- Aliberti, L., 2003. The evolution of the Earth's crust: a review. *Geological Society of America Bulletin* **105**, 15–31.
- Aliberti, L., 2003. Ophiolites. In: L. Aliberti (ed.), *Ophiolites*, 1–11.
- Aliberti, L., & Sartori, M., 2003. The evolution of the Earth's crust: a review. *Geology* **21**, 54–50.
- Aliberti, L., & Sartori, M., 2003. The evolution of the Earth's crust: a review. *Journal of Geological Society, London* **149**, 56–66.
- Aliberti, L., & Sartori, M., 2003. The evolution of the Earth's crust: a review. *Contributions to Mineralogy and Petrology* **86**, 54–66.
- Aliberti, L., & Sartori, M., 2003. The evolution of the Earth's crust: a review. *Ophiolites in Earth History* (ed. L. Aliberti & M. Sartori), 11, 43–61.
- Aliberti, L., & Sartori, M., 2011. The evolution of the Earth's crust: a review. *Geological Society of America Bulletin* **123**, 3–411.
- Aliberti, L., & Sartori, M., 2015. The evolution of the Earth's crust: a review. *Chinese Journal of Geology* **50**, 140–54 (in Chinese with English abstract).
- Aliberti, L., & Sartori, M., 2000. The evolution of the Earth's crust: a review. *Geodynamics* (ed. L. Aliberti), 1–11.
- Aliberti, L., & Sartori, M., 2000. The evolution of the Earth's crust: a review. *Contributions to Mineralogy and Petrology* **140**, 23–55.
- Aliberti, L., & Sartori, M., 2000. The evolution of the Earth's crust: a review. *Lithos* **27**, 25–55.

- Geological Bulletin of China 30, 150–153 (2011).

Geochimica et Cosmochimica Acta 75, 504–522 (2011).

Nature 410, 6–11 (2001).

Chemical Geology 182, 22–35 (2002).

Journal of Geophysical Research: Solid Earth (1978–2012) 101, 11–31 (2000).

Contributions to Mineralogy and Petrology 139, 20–26 (2000).

Geological Bulletin of China 31, 126 (2012).

Chinese Science Bulletin (Chinese Version) 59, 2213–2221 (2014).

Transactions of the Royal Society of Edinburgh: Earth Sciences 91, 1–13 (2000).

Journal of Petrology 31, 6–11 (2000).

Earth Science Frontier 10, 43–56 (2003).

Journal of Petrology 42, 655–671 (2001).

Nature 380, 23–40 (1996).

Tectonophysics 326, 255–266 (2000).

Proceedings of the Ocean Drilling Program, Scientific Results, vol. 176 (2010a).

Lithos 114, 1–15 (2010b).

Geological Magazine 141, 225–231 (2004).

Geostandards and Geoanalytical Research 34, 11–34 (2010).

Chinese Science Bulletin 58, 464–474 (2013).

Chinese Science Bulletin 55, 1535–1546 (2010).

User's Manual for Isoplot 3.00: A Geochronological Toolkit for Microsoft Excel (2003).

American Journal of Science 274, 32–355 (1994).

Geology 23, 51–54 (1995).

Structure of Ophiolites and Dynamics of Oceanic Lithosphere (2001).

Acta Petrologica Sinica 25, 16–24 (2009).

Acta Petrologica Sinica 25, 14–41 (2009).

Acta Petrologica Sinica 23, 162–172 (2007).

- 200 a. & . 2000. & . *International Journal of Earth Sciences* **98**, 11–21.

200 b. & . 2003. & . *American Journal of Sciences* **309**, 221–0.

1. 3. *Regional Geology of the Xinjiang Uygur Autonomous Region*. & . 11. 2 145().

2015. & . & . 2015. & . *Journal of Asian Earth Sciences* **113**, 5 .

2012. & . & . 2012. & . *Gondwana Research* **21**, 246–65.

200 . & . 2006. & . *Chemical Geology* **242**, 22–3.

2006. & . 2006. & . *Acta Geologica Sinica* **80**, 254–63().

& . 2003. & . 1 & . 1 & . *Chinese Science Bulletin* **48**, 2231–5.

. 2013. & . 1 & . & . 1 & . & . 1 & . *Lithos* **179**, 263–4.

. 2012. & . 1 & . & . 1 & . & . 1 & . *Journal of Asian Earth Sciences* **52**, 11–33.

200 . & . 200 . & . % & . & . & . 200 . & . & . & . *Acta Petrologica Sinica* **24**, 1054–5().

. & . 1. 6. & . & . % & . & . *Annual Review of Earth and Planetary Sciences* **14**, 43–51.